Single cell in vivo brain optogenetic stimulation by two-photon excitation fluorescence transfer

Lei Tong*[1], Peng Yuan*[1,2,#], Yao Xue[3], Minggang Chen[3], Fuyi Chen[1], Joerg Bewersdorf[5,6], Z. Jimmy Zhou[3,4,7], Jaime Grutzendler[1,4.#]

1, Department of Neurology, Yale School of Medicine, New Haven, CT, 06511

2, Department of Rehabilitation Medicine, Huashan Hospital, State Key Laboratory of Medical Neurobiology, Institute for Translational Brain Research, MOE Frontiers Center for Brain Science, Fudan University, Shanghai 200032, China

3, Department of Ophthalmology and Visual Science, Yale School of Medicine, New Haven, CT, 06511

4, Department of Neuroscience, Yale School of Medicine, New Haven, CT, 06511

5, Department of Cell Biology, Yale School of Medicine, New Haven, CT, 06511

6, Department of Biomedical Engineering, Yale University, New Haven, CT, 06511

7. Department of Cellular and Molecular Physiology, Yale University, New Haven, CT, 06511

*, authors contributed equally to this work

#, corresponding author

Abstract

Optogenetic manipulation with single-cell resolution can be achieved by two-photon excitation; however, this frequently requires relatively high laser powers or holographic illumination. Here we developed a practical strategy to improve the efficiency of two-photon stimulation by positioning fluorescent proteins or small fluorescent molecules with high two-photon cross-sections in the vicinity of opsins. This generates a highly localized source of endogenous single-photon illumination that can be tailored to match the optimal opsin absorbance. Through neuronal and vascular stimulation in the live mouse brain, we demonstrate the utility of this technique to achieve more efficient opsin stimulation, without loss of cellular resolution. We also provide a theoretical framework for understanding the potential advantages and constrains of this methodology, with suggestions for future improvements. Altogether, this fluorescence transfer illumination method allows experiments difficult to implement in the live brain such as all-optical neural interrogation and control of regional cerebral blood flow.

Introduction

Optogenetics with light-sensitive opsins has revolutionized the field of neuroscience (1). Typical experiments involve the utilization of single-photon illumination of the brain to activate opsins such as channelrhodopsin (ChR2) and others (2). While this allows temporally precise manipulation of cell ensembles, all the cells along the conical illumination light path are activated, reducing the spatial specificity and resulting in artificially synchronized activity patterns (3). These drawbacks limit the application of optogenetics to answer important questions involving manipulation of specific cells such as neurons and other excitable cells like vascular smooth muscle cells and astrocytes, within ensembles. In order to overcome these limitations, it is desirable to achieve optogenetic stimulation with single-cell level precision. One approach is to utilize two-photon absorption, which is characterized by being limited to the immediate vicinity of the focal point, thereby achieving spatially restricted activation of opsin channels (3). Several studies have demonstrated the feasibility of this approach (4-12); however, two-photon optogenetics has relatively low efficiency in eliciting a biological response, which limits its *in vivo* applications (**Figure 1**).

One of the reasons for its low efficiency is that the two-photon effect occurs in a submicron focal volume (13). Thus, only a small patch of cell membrane is illuminated at any point in time during laser scanning, which limits the number of opsin molecules that are synchronously stimulated. This limits the ion flux necessary to induce changes in membrane potential and the resulting ability to trigger action potentials. Opsin stimulation can be improved by the use of higher laser power, but unfortunately this can also have direct effects on membrane potential and cell excitability (14-16), likely due to two-photon thermal effects (17, 18), which can cause confounding opsin- or activity-independent ion channel opening. Furthermore, the use of high laser power is problematic as it may induce a variety of cell signaling changes and toxicity (19-21). An alternative to improve the efficiency of two-photon illumination is to use fast laser scanning and generate spiral paths that roughly match the cell's

53 perimeter, which allows nearly simultaneous activation of a larger number of opsin channels along the
54 cellular membrane (4, 9). A related technique uses spatial light modulators to generate a hologram in
55 the sample so that the laser can simultaneously illuminate the entire target cell (12, 22, 23) and thereby
56 elicit a more robust cellular response. While studies have demonstrated *in vivo* manipulation of neural
57 activity at single-cell resolution with both techniques (24-27), they require advanced optics and complex
58 instrument operation that limit their implementation by most researchers. Thus, it would be of great
59 utility to improve the efficiency by which opsins are stimulated with conventional two-photon
60 illumination and thereby achieve reduced laser scanning times and power requirements. Here we
61 propose a robust and practical approach to achieve *in vivo* optogenetic control of single cells that we
62 termed two-photon excitation fluorescence transfer (TEFT). This approach markedly improves the
63 efficiency of targeted optogenetic control of excitable cells in the live brain and should be entirely
64 compatible with current methodologies including spiral cell scanning and holographic illumination,
65 commonly used for studies of brain networks, cell physiology and neurovascular coupling.

66 **Results**

67 **Two-photon excitation fluorescence transfer (TEFT) for in vivo optogenetics**

68 In conventional two-photon optogenetics, opsins located in a small patch of membrane defined by the
69 width of the diffraction-limited point-spread-function (PSF) (hundreds of nanometers diameter) are
70 activated at any point in time, leading to relatively inefficient stimulation of the cell (9). Instead of
71 directly activating the light-sensitive opsin channels on the cell membrane, TEFT utilizes the two-photon
72 laser to excite fluorophores located in the vicinity of the opsins. These fluorophores have a fluorescence
73 emission spectrum matching the optimal (single-photon) opsin absorption, which is now used instead of
74 two-photon excitation, to indirectly stimulate opsins in the target cell **(Figure 1)**. Effectively, this
75 converts two-photon stimulation into a local single-photon point source that can be efficiently used for

76 optogenetics (9)(**Figure 2**). In addition, with TEFT, fluorescent molecules can be selected for a high two-
77 photon cross section and high quantum yield that better matches the adjacent opsin excitation
78 properties. Importantly, one can control the concentration of either small fluorophores or fluorescent
79 proteins and their location (i.e. cell cytoplasm or intravascular space) and excite the full volume of the
80 PSF which is much greater than the amount of membrane bound opsins that are normally excited by
81 direct two photon illumination. This translates into a more efficient single-photon illumination point
82 source that can stimulate larger areas of the adjacent cell membranes. While the total amount of
83 fluorescence is determined by the focal excitation, the light intensity that reaches the membrane-bound
84 opsins decays with the inverse square of the distance from the focal point. We further calculated two
85 forms of excitation crosstalk: 1) The out of focus two-photon excitation of a neighbor cell at a different
86 axial position (**Figure 2h**); and 2) The activation of a neighbor cell from the target cell's fluorescence
87 (**Figure 2i** and **Supplementary Figure 1**). Our calculation shows that the activation of a neighbor cell can
88 only reach up to a maximum of 10% of that of the target cells. This provides a theoretical framework for
89 understanding the ability of TEFT for efficient optogenetic stimulation without a loss of single cell
90 resolution (**Figure 2**).

91 **In vivo optogenetic control of vascular smooth muscle cells with TEFT stimulation**

92 Guided by the abovementioned TEFT optogenetics principles, we tested the feasibility of two-photon
93 optogenetic stimulation of vascular smooth muscle cells (vSMC) in the live mouse brain to locally control
94 cerebral blood flow (28). Optogenetic control of the brain vasculature has recently been implemented as
95 a powerful tool for dissecting mechanisms of neurovascular coupling and its control by different
96 vascular mural cell types (29-31). We hypothesized that TEFT may improve the efficiency and reliability
97 of vascular optogenetics, and thus investigated this method with various combinations of opsins and
98 intravascular fluorescent dyes as previously described (32). We first tested the ability to induce vessel
99 constriction in Cspg4-Ai32 mice, in which the perivascular vSMCs express the excitatory ChR2. In order

100 to provide the fluorescence emission that matches the optimal absorption of ChR2, we intravascularly
101 injected cascade blue-conjugated albumin. We then scanned a region of interest (ROI) over the selected
102 vessel segment using the femtosecond laser tuned to 800 nm, a wavelength that is suboptimal to
103 directly excite ChR2 (33) and therefore cannot induce adequate vSMC contraction (**Figure 3**). As
104 predicted, we observed a robust vessel constriction that was only elicited when we implemented the
105 stimulation in the presence of intravascular cascade blue (**Figure 3a, Supplementary Movie 1**). In
106 contrast, we did not observe any vessel constriction when we used an unconjugated control albumin,
107 albumin conjugated with a dye not optimally matched to ChR2 absorption (**Figure 3d**) or when we used
108 a 950-nm wavelength, which does not excite the cascade blue dye (**Figure 3e**). Importantly, the
109 stimulation only induced constriction of the targeted vessel segments, while the diameter of adjacent
110 segments or vessels in the nearby region remained unchanged (**Figure 3g** and **Supplementary Figure 3**).
111 Next, we used archaerhodopsin (Arch)-expressing mice (Cspg4-ArchT (Ai40D)) to induce vSMC
112 hyperpolarization and determine the efficiency of TEFT to induce vSMC-relaxation and consequent
113 vasodilation. To achieve the optimal single-photon activation wavelength of Arch (~545 nm, (34)), we
114 utilized an intravascular Alexa514-conjugated albumin and 900-nm two-photon illumination. This
115 resulted in efficient and focal vessel dilation (**Supplementary Movie 2**), which did not occur in the
116 absence of the intravascular dye (**Figure 4a and b**). For both ChR2 and ArchT activation, we found that
117 many other dyes with similar emissions were capable of inducing opsin activation. For example, all three
118 blue-emitting fluorescent dyes, Cascade-blue, Alexa 405 and AMCA (aminomethylcoumarin acetate),
119 were able to trigger vessel contraction in Cspg4-ChR2 mice (**Figure 3f**), while the two yellow-emitting
120 dyes, Alexa 514 and Lucifer yellow, produced vessel dilation in Cspg4-ArchT mice (**Figure 4e**). Together,
121 these results demonstrate that the fluorescence generated from these intravascular dyes by two-photon
122 excitation was a potent indirect light source for highly efficient and specific optogenetic control of
123 vSMCs *in vivo*.

124 **Improved efficiency of two-photon optogenetics in neurons by TEFT**

125 Having demonstrated the effectiveness of TEFT using intravascular dyes to activate vSMCs, we next
126 explored the feasibility of applying this method to neurons. In order to measure the efficiency of
127 optogenetics, we performed patch-clamp recordings of pyramidal neurons in acute mouse brain slices
128 (**Figure 5**). We implemented TEFT, by expressing ReaChR in neurons (through *in utero* electroporation)
129 and filling the recording electrode with Alexa594 solution (**Figure 5a**). To achieve optogenetic
130 stimulation, we scanned these cells by two-photon illumination of a ROI covering the entire cell body
131 using a wavelength of 800 nm for ~50 ms. We found that adding the dye increased the peak current by
132 ~50%, compared to cells with no dye, under the same laser stimulation conditions (**Figure 5b and c**). In
133 addition, TEFT-mediated activation showed faster onset kinetics compared to direct two-photon
134 optogenetics (**Figure 5d**), consistent with the TEFT principle, that all opsins on the target cell were
135 activated simultaneously, rather than sequentially as is the case with direct two-photon membrane-
136 opsin activation.

137 We next applied TEFT in the live brain. Due to the difficulty of introducing organic fluorescent
138 dyes into cells *in vivo*, we instead overexpressed fluorescent proteins in the target neurons. We used *in*
139 *utero* electroporation of neurons in the mouse brain to first co-express the red-emitting fluorescent
140 protein tdTomato and the opsin ReaChR (peak absorption 595 nm), as well as the calcium sensor
141 GCaMP6 to detect neuronal activity changes. To test the feasibility of implementing TEFT in neurons, we
142 scanned these cells by two-photon illumination of a ROI covering the entire cell body using a wavelength
143 of 920 nm, which has been reported to excite ReaChR (35). This focused scanning triggered a rapid rise
144 in GCaMP6 fluorescence (**Figure 5e and f**).

145 We then compared this optogenetic-induced calcium rise in cells with and without tdTomato co-
146 expression. While two-photon scanning can directly stimulate ReaChR at relatively high powers (35), co-

147 expression with tdTomato markedly increased the efficiency, and enabled activation with laser powers
148 that are normally too low for ReaChR stimulation (**Figure 5g**). We observed ~50% reduction of the laser
149 power required to reach 50% probability of activation using the TEFT method (**Figure 5h**). Importantly,
150 TEFT improves the efficiency of cell activation while maintaining the single-cell resolution, since we
151 could elicit a robust calcium rise in the targeted cell, without any calcium changes in the immediately
152 adjacent one (**Supplementary Figure 3a-c**). Together, these observations demonstrate that TEFT-
153 mediated two-photon optogenetics improves the efficiency of cell activation.

154 **Fluorophore/opsin constraints critical for optimal TEFT efficiency**

155 In contrast to the tdTomato/ReaChR pair for TEFT optogenetic stimulation, we were not able to elicit
156 two-photon activation of ChR2 when pairing it with genetically encoded blue fluorescent proteins or
157 SNAPtag-targeted organic dyes co-expressed in the same neurons (**Supplementary Figure 4**). This
158 contrasts with the highly efficient activation we observed when ChR2 in vSMCs was stimulated in the
159 presence of blue intravascular organic dyes (**Figure 2**). As an explanation for this phenomenon, we
160 hypothesized that the number of photons emitted by the donor fluorophores in the vicinity of opsins is a
161 critical variable that determines their efficient activation. To better understand this relationship, we
162 calculated the theoretical number of photons emitted after two-photon excitation of various well-
163 known fluorescent proteins (36, 37)(**Figure 2 and Supplementary Figure 4c**). With these data, we
164 determined that the mTagBFP/ChR2 pair that we used experimentally for neurons, was not suitable for
165 TEFT optogenetics, given that for laser powers of ~10 mW, typical of most intravital applications, the
166 calculated emitted fluorescence of mTagBFP was only of the order of 0.01 mW/mm^2, which is two
167 orders of magnitude lower than the reported power needed for ChR2 activation (38). In contrast, with
168 the tdTomato/ReaChR pair, using 10 mW for two-photon illumination, yielded around 0.15 mW/mm^2
169 (**Supplementary Figure 4d**), which is known to be sufficient to elicit strong ReaChR photocurrents (39).
170 One way to overcome the low two-photon cross section of most genetically encoded blue fluorescent

171 proteins, would be to increase their intracellular concentration to achieve greater net photon emissions.
172 However, it is difficult to increase their intracellular concentrations beyond ~10 micromolar (40). This
173 contrasts with the concentration of intravascular dyes that we used for stimulation of ChR2 in vSMCs
174 (~500 micromolar), which can be further increased as needed, thereby achieving highly efficient TEFT
175 optogenetic stimulation.

176 **Discussion**

177 Here we reported a novel approach to improve the limited efficiency of two-photon illumination for
178 opsin stimulation *in vivo*. By positioning organic dyes or genetically encoded fluorescent proteins in the
179 cytoplasm or immediate vicinity of opsins (intravascular), and using two-photon illumination to excite
180 them, a focal source of single-photon emissions is generated, which efficiently activates adjacent opsins.
181 The TEFT technique retains the focal illumination properties (given the rapid intensity decay as a
182 function of distance from the single-photon light source, see **Figure 2**), which allows opsin stimulation at
183 cellular and possibly subcellular resolution. Interestingly, our calculation showed that TEFT has a low
184 (<7%) cross-talk illumination power to the neighbor cell, across different sizes of the target cell (**Figure2**
185 and **Supp. Figure 1**). Together with the fact that the effective illumination power is higher in smaller
186 structures (inversely correlated with surface area, **Figure 2**), TEFT may provide an ideal method for
187 optogenetic experiments requiring high resolution such as those of single dendritic spines. We
188 demonstrated that TEFT improves the efficiency of *in vivo* experiments otherwise not easily achievable
189 such as targeted opsin stimulation of vSMCs and neurons with widely available standard two-photon
190 microscopy setups. The lower laser power requirements achieved by this method could be critical for
191 reducing thermal injury (41) and unwanted laser-induced electrophysiological effects independent of
192 opsin activation (14, 16). TEFT can be further optimized in the future by improving the quantum yield of
193 the paired fluorescent proteins utilized or by developing more efficient methods for targeting bright
194 organic dyes to specific cellular compartments, thereby achieving higher *in vivo* concentrations. Finally,

195 this method is entirely compatible and should also improve the efficiency of other methods for two-
196 photon optogenetic stimulation such as the use of fast spiral scanning paths (4, 9) or scanless
197 holographic approaches (22, 23). Together our data demonstrates a significant improvement in the
198 methodologies for targeted cell optogenetics stimulation that are critical for experiments requiring
199 precise spatial and temporal single-cell stimulation for investigation of cellular physiology and neural
200 networks *in vivo*.

201

202 **Figures and figure legends**

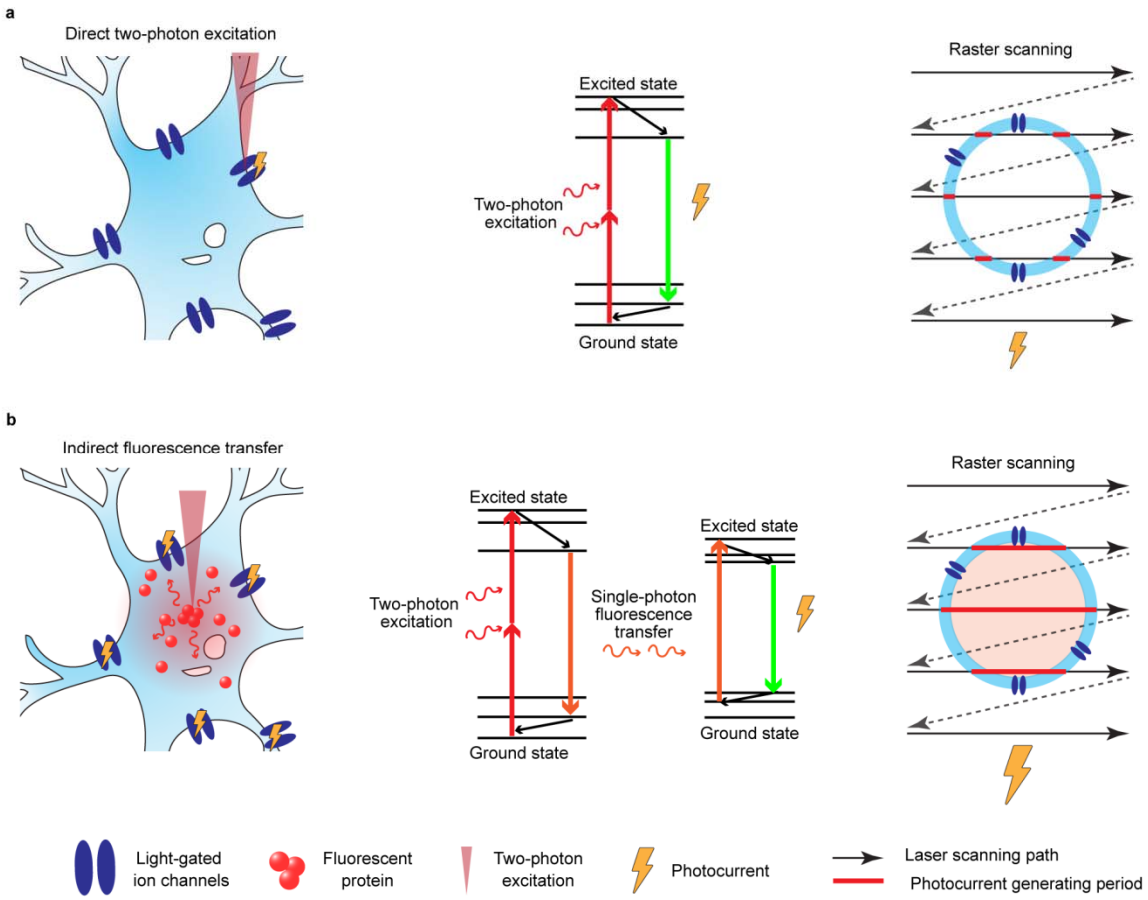

203
204 **Figure 1: Diagram depicting the principle of two-photon excitation fluorescence transfer (TEFT).** (**a**)
205 Direct two photon illumination of light gated ion channels (opsins) induces photocurrents mainly at focal
206 points on the cell membrane as the laser scans the field of view (left diagram). Jablonski diagram
207 depicting standard two photon excitation of opsins and resulting photocurrent (Middle diagram). Raster
208 scanning showing opsin activation at site of focal membrane illumination by two-photon laser (Right
209 diagram). (**b**) Expression of fluorescent proteins or presence of organic dyes in the immediate vicinity of
210 opsins (i.e. cell cytoplasm or intravascular space) allows indirect two-photon illumination (Left diagram)
211 by scanning the entire area and exciting fluorophores all along the path instead of just at sites of opsins
212 on the membrane (Right diagram). The two-photon excitation of adjacent fluorophores generates single
213 photon emissions that are less focal and can indirectly activate the adjacent membrane opsins and
214 generate photocurrents. This can improve the efficiency of opsin activation because it generates a larger
215 number of exciting photons, thereby more efficiently stimulating the adjacent opsins.

216

217

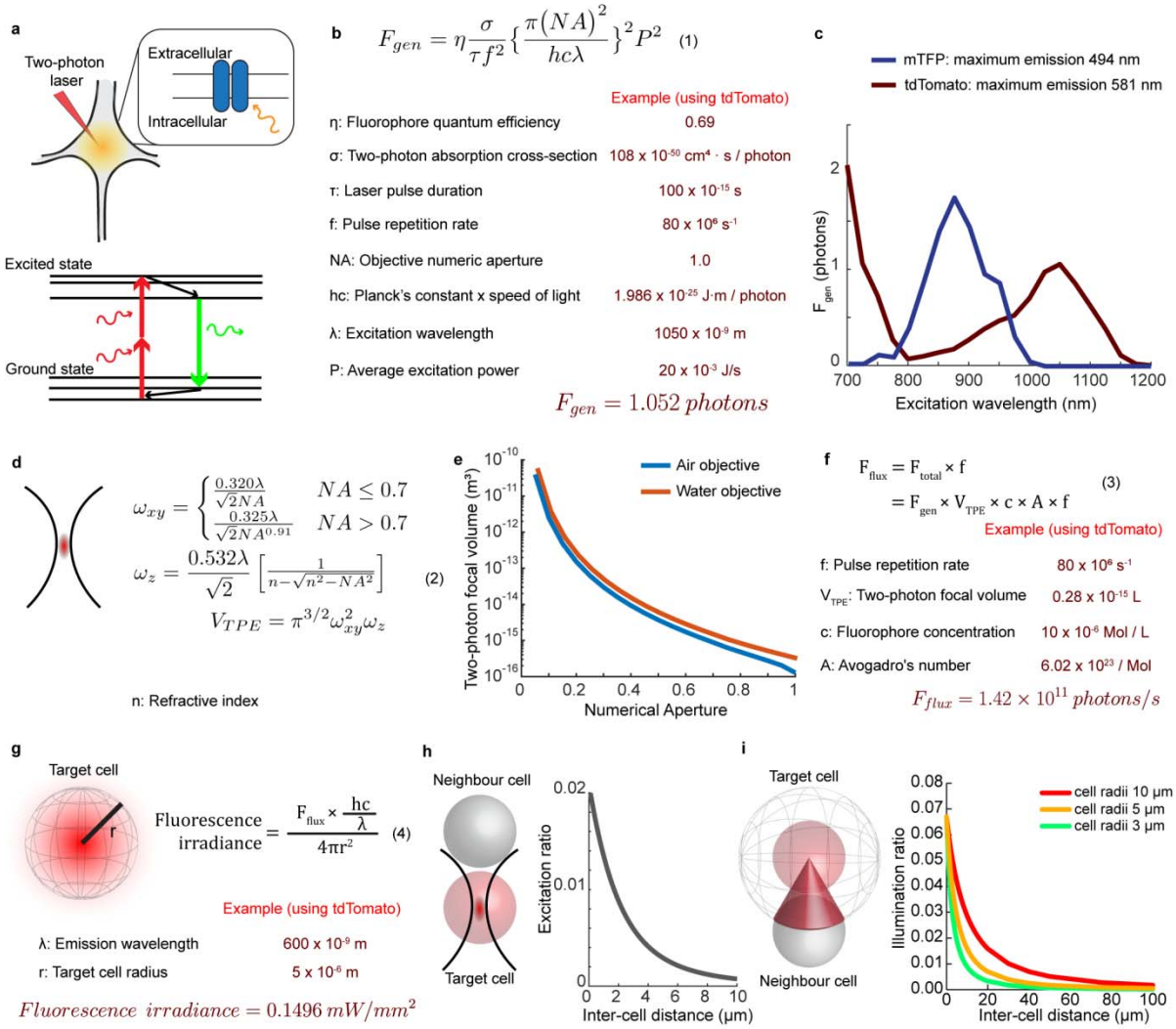

Figure 2: Theoretical estimation of fluorescence irradiance with two-photon excitation. (**a**) Schematic diagram of fluorescence transfer mediated two-photon optogenetics and the Jablonski diagram for the principle of two-photon excitation. Two-photon excitation generates fluorescence that can be absorbed by opsins expressed on the cell membrane. Two prerequisites for efficient fluorescence transfer optogenetics: 1, matching the spectrum between fluorophore emission and opsin absorption; and 2, sufficient irradiance of the fluorescence to generate photocurrents. (**b**) Equations describing the photons generated per fluorophore per pulse (modified from (13)). (**c**) Simulation of two-photon excited fluorescent photon for mTFP and tdTomato at different excitation wavelengths. (**d**) Equations estimating two-photon focal volume (modified from (42)). (**e**) Theoretical calculation of two-photon focal volume at 1050 nm, with air or water objective at different numerical aperture configurations. (**f**) Equations estimating total fluorescence flux. (**g**) Equations estimating fluorescence irradiance to the cell surface. (**h**) Estimation of axial off-target two-photon activation. The plot on the right shows the excitation ratio between the neighbour cell and the target cell at different distances. **(i)** Theoretical estimation of fluorescence transfer efficiency to a non-target cell. The ratio of fluorescence radiation to the target cell (red) and to a non-target neighbor cell (grey) can be expressed as the ratio between the spherical cone

234 cap area to the total sphere area. The plot on the right shows the theoretical calculations of illumination
235 ratios between the target and neighbour cells at different sizes and distances.

236

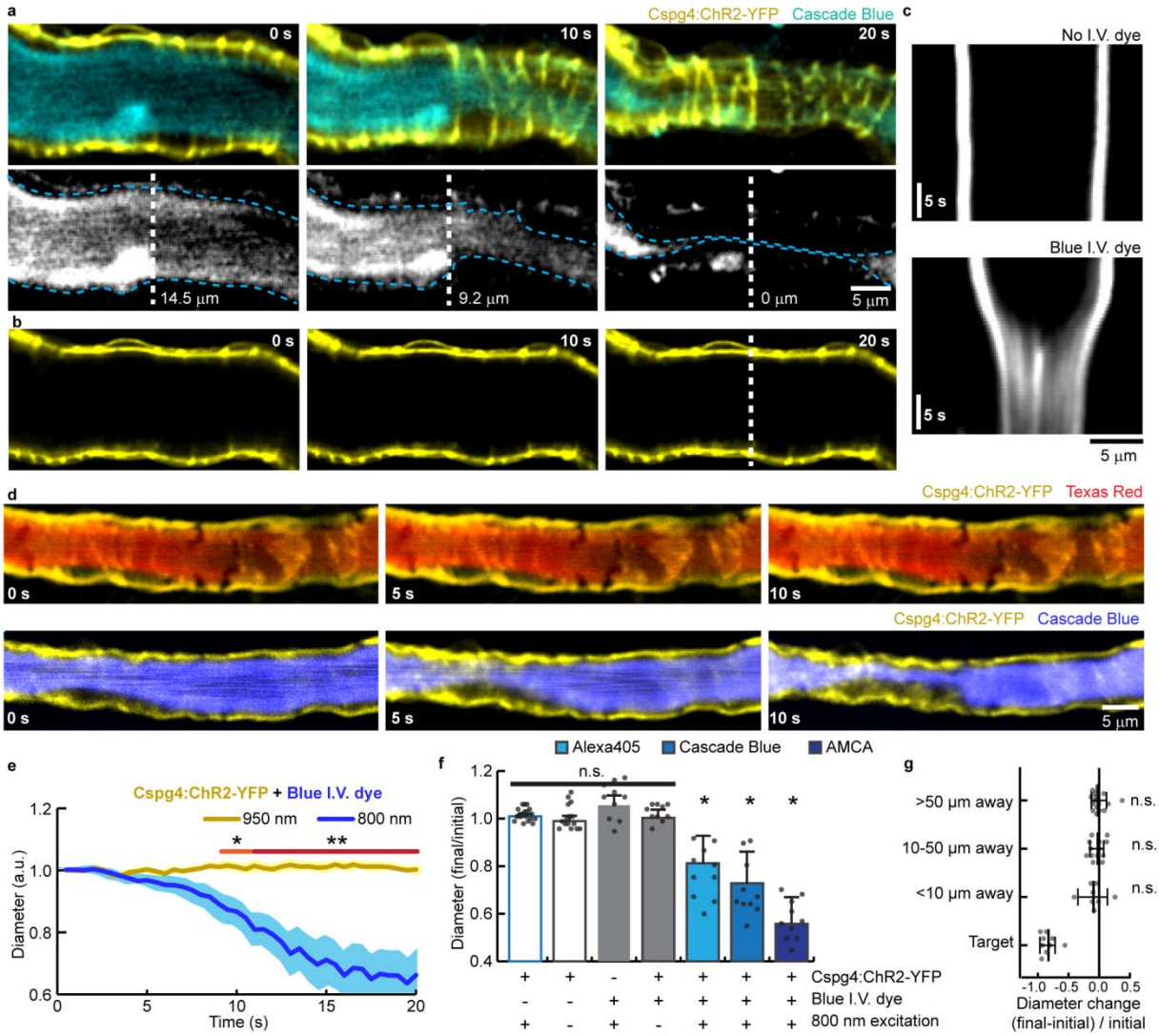

Figure 3: Fluorescence transfer-mediated two-photon optogenetic excitation of vascular smooth muscle cells in vivo. (**a**) Time-lapse intravital brain imaging in mice expressing ChR2 in vascular smooth muscle cells (Cspg4:ChR2-YFP) show focal vessel constriction induced by two-photon illumination of intravascular blue dye (cascade blue). Blue dashed lines (lower row) show the outlines of the intravascular space (cross-section widths indicated by white dashed lines). (**b**) Time-lapse images of the same vessel segment as in **a,** without the intravascular blue dye, showing no changes in diameter with the same laser power. Scanning parameters in **a** and **b**: 25 Hz, 800 nm laser, 10 µs dwell time, 10mW. (**c**) Vessel cross-sections during the scanning periods at the locations of white dashed lines in **a** and **b**. (**d**) Two-photon time-lapse intravital images of optogenetic stimulation in a Cspg4-cre:Ai32 mouse with a red intravascular dye show little change in diameter (upper row), while the same vessel segment with a blue intravascular dye demonstrates robust constriction (lower row). (**e**) Quantification of normalized vessel diameters during two-photon scanning at 800nm and 950nm wavelengths. Data are represented as mean ± standard deviation. N=10 vessels for each group. Orange and red segments indicate statistically significant timepoints between groups (*: $p<0.05$ and **: $p<0.01$, respectively, Student's t-test between groups for each time points, with Bonferroni's correction for multiple comparisons). (**f**)

Quantifications of vessel diameters at the end of the stimulation with different experimental conditions. Data are presented as mean ± standard deviation, with individual datapoints provided (N=10 to 20 vessels per group). One sample Wilcoxon tests were used for each group to compare to 1, with additional Bonferroni's correction for multiple comparisons (*: $p<0.05$). (**g**) Quantification of vessel diameter changes between the start and the end of TEFT stimulation in the vessel segments at different distances to the target region. Data are presented as mean ± standard deviation, with individual datapoints provided (N=10 to 20 vessels per group). One sample Wilcoxon tests were used for each group to compare to 0.

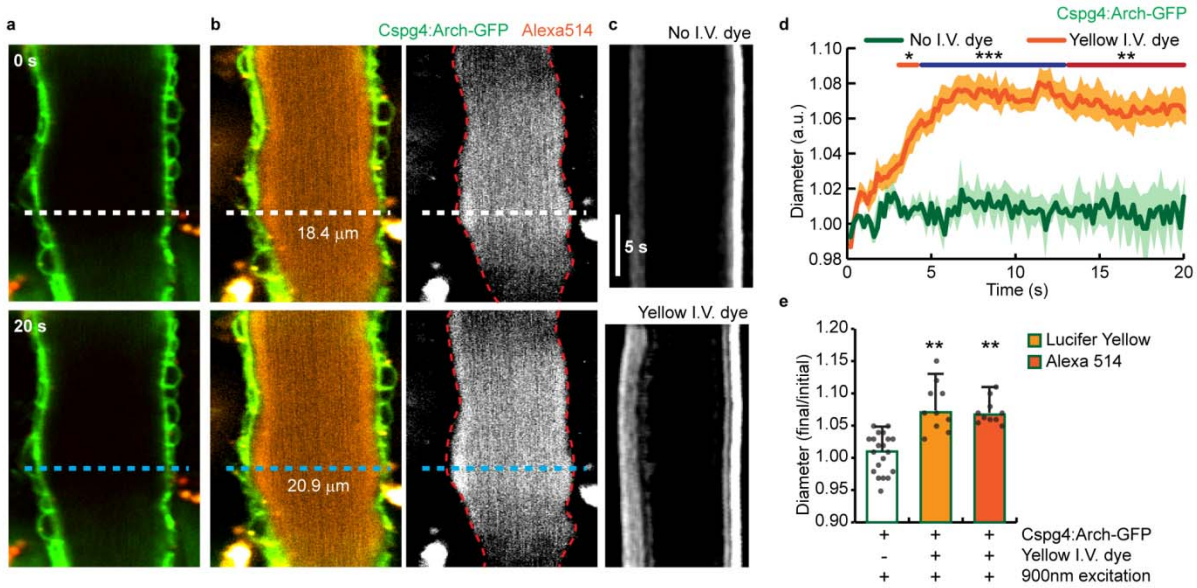

Figure 4: Fluorescence transfer-mediated two-photon optogenetic inhibition of vascular smooth muscle cells in vivo. (**a**) Two-photon time-lapse images of vessel dilation in archaerhodopsin expressing mouse (Cspg4:ArchT-GFP). (**b**) Representative two-photon time-lapse images of the same vessel segment with yellow intravascular dye. White and blue dashed lines show site where diameter was measure overtime in **a** and **b**. Scanning parameters in **a** and **b**: 25 Hz, 900 nm laser, 10 µs dwell time, 10mW. (**c**) Vessel cross-section line profiles depicted overtime during scanning at the locations of dashed lines in **a** and **b**. (**d**) Quantification of normalized vessel diameters with and without yellow intravascular dye. Data are represented as mean ± standard deviation. N=10 vessels per group. Yellow, red and blue segments indicate statistically significant timepoints between groups (*: $p<0.05$; **: $p<0.01$ and ***: $p<0.001$, respectively, Student's t-test between groups for each time point, with Bonferroni's correction for multiple comparison). (**e**) Quantification of vessel diameters with different experimental conditions. Data are presented as mean ± standard deviation, with individual datapoints provided. N=10 to 20 vessels per group. One sample Wilcoxon tests were used for each group to compare to 1, with additional Bonferroni's correction for multiple comparison (**: $p<0.01$).

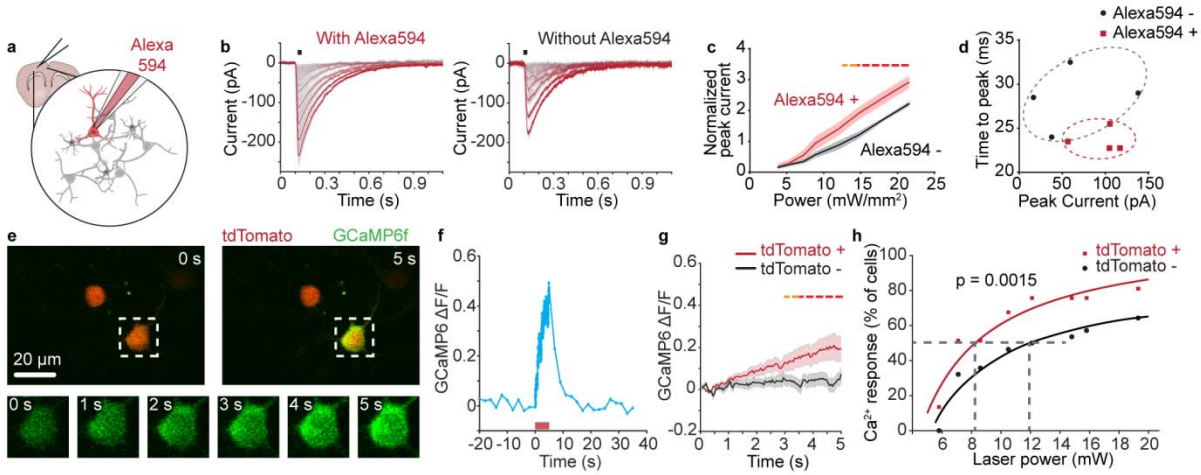

Figure 5: In vivo optogenetics of single neurons using fluorescence transfer-mediated two-photon stimulation. (**a**) Schematics of patch clamp recording with TEFT. (**b**) Representative traces of two-photon elicited currents in cells with or without Alexa594 dye at 800 nm. Laser powers are 3.8, 5.4, 7.3, 8.9, 12, 14.8, 18.1 and 21.6 mW, for curves from grey color to red. Black lines indicate a 50 ms two-photon stimulation period. (**c**) Quantification of the peak current amplitudes in cells with or without Alexa594 dye, normalized by the peak current recorded at 920 nm at 5 mW. N = 4 cells in each group. Data are represented as mean ± standard error (Student's t-test comparison between groups for each time point, a false discovery rate of 5% was set for multiple comparison correction. Yellow dash lines: $p<0.05$, red dash lines: $p<0.001$) (**d**) Quantification of onset phase kinetics of two-photon activated currents in cells with or without Alexa594 dye, plotted against peak currents. Dash lines indicate the perimeter for each condition group. (**e**) Two-photon raster scanning in a live mouse brain of ROI (white dashed square) covering a neuron that is co-expressing ReaChR, GCaMP6 and tdTomato, induces robust calcium transients (ROI scan parameters: pixel size: 0.42 µm/pixel, 50 Hz, 5 s, 920 nm laser, 4 µs dwell time, 8.6 mW). Time-lapse images (bottom panel, green) show rapid increase in calcium levels following two-photon illumination. (**f**) GCaMP6 calcium response of a neuron coexpressing ReaChR, GCaMP6 and tdTomato using the same scanning parameters as in **e** (ROI scanning interval indicated by the orange bar). (**g**) Comparison of two-photon optogenetics in ReaChR/GCaMP6 positive neurons with and without tdTomato expression at 8.6 mW excitation power (N=37 for tdTomato positive; N=28 for tdTomato negative). Data are represented as mean ± standard error (Student's t-test comparison between groups for each time point, a false discovery rate of 5% was set for multiple comparison correction. Yellow dash lines: $p<0.05$, red dash lines: $p<0.001$). (**h**) GCaMP6 responses by 920nm two-photon activation of ReaChR in cells with and without the expression of tdTomato. Curve fitting showed that tdTomato-expressing neurons are more efficiently activated than tdTomato-negative neurons at various laser powers (20% rise of GCaMP6 fluorescence used as arbitrary threshold of neuronal activation) ($p=0.0015$ comparing differences between fitted curves, see methods for statistical details).

306 **Supplementary Movie 1: Fluorescence transfer-mediated two-photon optogenetic activation of ChR2**
307 **in vascular smooth muscle cells leads to vessel constriction.** Time-lapse videos of the same vessel
308 segment in a Cspg4-Ai32 mouse with (right panel, 800nm excitation) and without (left panel, 925nm
309 excitation) the excitation of the intravascular blue-emitting dye. Scanning parameters in both: 25 Hz, 10
310 µs dwell time, 10mW laser power.

311 **Supplementary Movie 2: Fluorescence transfer-mediated two-photon optogenetic activation of ArchT**
312 **in vascular smooth muscle cells leads to vessel dilation.** Time-lapse videos of the same vessel segment
313 in a Cspg4-Ai40D mouse with (right panel, 900nm excitation) and without (left panel, 930nm excitation)
314 the excitation of the intravascular yellow-emitting dye. Scanning parameters in both: 25 Hz, 10 µs dwell
315 time, 10mW laser power.

316 **Materials and Methods**

317 **Mice**

318 All rodent procedures were approved by the Yale University Institutional Animal Care and Use
319 Committee. For vascular studies, transgenic mice that express the Cre recombinase under the mural cell
320 NG2 (Cspg4) promoter, and reporter lines with cre-dependent channelrhodopsin-2 (Ai32) or
321 Archaerhodopsin-3 (Ai40D) were purchased from The Jackson Laboratory (JAX# 008533, JAX# 021188,
322 JAX# 012569). Cre-expressing strains were crossbred with the reporter strains and the offspring were
323 used for all experiments. For neuronal studies, wild type mice were used for electroporation of various
324 constructs (JAX# 000651). For all experiments, 2-3-month-old mice from both sexes were used.

325 **Reagents**

326 Purified albumin (Sigma-Aldrich, 05470) was used for fluorescent dye conjugation. Reactive esters were
327 used for labeling (Thermo Fisher Scientific, C-2284, A6118, A30000, L-1338) according to the
328 manufacturer's instruction. The labeled albumin was diluted so that 5mg reactive dyes constituted 1mL
329 of injection stock. 100µl of labeled albumin was injected intravenously before imaging, final dye
330 concentration in blood was estimated to be ~0.5mM. In all conjugations, albumin was used at
331 concentrations greater than the number of fluorophores to eliminate the need for free fluorophore
332 purification.

333 To express constructs by in Utero electroporation we obtained and modified the following plasmid
334 constructs from Addgene: CAG-tdTomato, CAG-ReaChR (#50954), Syn-GCaMP6f (#100837), CAG-tagBFP
335 (#49151), Syn-ChR2 (#58880), CAG-jRCaMP (#61562). See **Supplement** for maps of modified plasmids.

336 **In utero electroporation**

337 In utero electroporation was done as previously described (43). Briefly, Plasmids were used at the final
338 concentration of 1.0 µg/µl (for each plasmid), mixed with 2 mg/ml Fast Green for visualization during
339 plasmid injection and electroporation. Electroporation was performed around embryonic day 13 to 15
340 (E13 to E15). Mice were anesthetized with ketamine/xylazine (100mg/kg and 10mg/kg i.p.).
341 Buprenorphine was administered (i.p.) every 12 hours for 2 more days following surgery. After exposing
342 the uterine horns, ~1 µl of plasmid mixture was pressure injected into the lateral ventricle of each
343 embryo via a pulled glass microelectrode (tip size 10~20 um) using Picospritzer II (General Valve, 20 psi).
344 50 V current pulses generated by a BTX 8300 pulse generator (BTX Harvard Apparatus) were used for
345 electroporation. Mice were allowed to age to 1 month prior to utilization in all experiments.

346 In order to verify the co-expression of tdTomato, ReaChR and GCaMP6, we used in vivo two-photon
347 imaging to monitor the cells while shining a red LED to trigger ReaChR activation, triple positive cells
348 should have baseline red fluorescent signal and a LED-triggered green fluorescent signal. The co-
349 expression probability was very high with electroporation. And only cells that demonstrated robust
350 triple expression were then targeted for two-photon stimulation.

351

352 **Craniotomy surgery, window implantation and in vivo two-photon imaging**

353 Mice were anesthetized with an intraperitoneal injection of Ketamine/Xylazine mixture, with final
354 concentration of 100mg/kg and 10mg/kg, respectively. The status of anesthesia was assessed

355 periodically with hind paw pinch. The mouse was head-fixed to a custom-made headplate by gluing the
356 skull to it. A craniotomy of about 4mm diameter was made (AP -1.5mm, ML 2.0 mm) with a dental drill,
357 with dura mater carefully removed. A coverslip was put to cover the craniotomy opening and secured
358 with cyanoacrylate glue. The mouse was kept anesthetized during subsequent imaging sessions, and
359 immediately euthanized after finalizing the experiment.

360 Two-photon imaging was carried out with a commercial system (Bruker Ultima Investigator), controlled
361 through Prairie View software. A tunable Ti:Sapphire laser was used to generate two-photon excitation
362 with its wavelength and mode-locking tuned through MaiTai software. In the case of RCaMP imaging, a
363 1045nm fixed wavelength laser (MaiTai InSight X3) was used. A pockels cell was used to modulate laser
364 power; and the laser power on the sample was measured with a power meter (Thorlabs PM100D). The
365 point scanning was achieved by galvanometer scanners with various dwell times. The full frame rate was
366 kept at 0.5 Hz, and for stimulation, the scanning within regions of interests (ROIs) was at 20 Hz or 50 Hz
367 frequencies. During ROI scanning, the regions outside the ROI were not scanned nor imaged
368 (represented by the dashed portion of the GCaMP6 response curved in **Figure 5**). Fluorescence emission
369 was collected with gallium arsenide phosphide photo-multiplier tubes. A 20x water immersion 1.0
370 numerical aperture objective (Zeiss) and a 10x air 0.4 numerical aperture objective (Leica) were used for
371 most experiments. For all in-vivo experiments, imaged blood-vessels were identified within 250 µm from
372 pia mater, and imaged neurons were located at depth between 100 to 350 µm. In all our experiments,
373 cells demonstrated normal spontaneous and stimulated responses, and showed no signs of persistently
374 elevated calcium levels associated with cell damage (44).

375 **Single cell patch clamp and two-photon optogenetics**

376 Acute brain slices of the in utero electroporated mice (P30-P40) were prepared following a N-methyl-D-
377 glucamine (NMDG) protective recovery method (45). Whole cell patch clamp and two-photon
378 optogenetics were then performed in slices in an ASCF containing (in mM) 120 NaCl, 3.1 KCl, 1.1 CaCl2,
379 1.2 MgCl2, 1.25 MgSO4,26 NaHCO3, 0.5 L-glutamine, 0.1 ascorbic acid, 0.1 Na-pyruvate, and 20 glucose;
380 saturated with 95% O2–5% CO2 at 35°C. To target fluorescent cells, we used a two-photon microscope
381 system (Ultima; Prairie Technologies) equipped with a Ti:Sapphire pulsed laser (MaiTai), configured on
382 an Olympus upright microscope (BX51WI) with a 20×, 0.5 NA objective lens (LUMPlanFL/IR) and a 60x,
383 1.0 NA objective lens(LUMPLANFL/IR). Cells were patched under 60x objective lens with pipette
384 solutions as follows (in mM): (1) for voltage clamp, 105 CsMeSO4, 0.5 CaCl2,10 HEPES, 5 EGTA, 5 Na2-
385 phosphocreatine, 2 ATP-Mg, 0.5 GTP-2Na, 2 ascorbic acid, and 8 QX314-Cl (pH 7.2), with 20–30 CsOH; (2)
386 for current clamp, 105 potassium gluconate, 5 KCl, 0.5 CaCl2, 2 MgCl2, 5 EGTA, 10 HEPES, 5 Na2-
387 phosphocreatine, 2 ATP-2Na, 0.5 GTP-2Na, and 2 ascorbic acid (pH 7.2) with 5 NaOH and 15 KOH. Liquid
388 junction potential was calculated with pCLAMP software and corrected (Molecular Devices, Union City,
389 CA). Once whole cell patch clamp was achieved, 20x objective lens was switched for two-photon
390 optogenetics. A single ROI (~10 x 10 µm) including only the cell soma was chosen for raster scan, with 4
391 µs dwell time, and laser intensity less than 25 mW (3.8, 5.4, 7.3, 8.9, 12, 14.8, 18.1 and 21.6 mW), which
392 shows no clear photo damage to cell membranes. 800 nm wavelength was used to excite intracellular
393 dye (Alexa 594, 0.5 mM). The photocurrent under 920 nm, which would not activate Alexa 594(46) was
394 also recorded to evaluate the expression level of ReaChR. An external voltage was used to trigger the
395 two-photon image scan, so that the timing of laser scanning and cell voltage/current can be accurately
396 matched for later analysis. The raster scanning was started at 0.1 s in each trail and last for 50 ms.

397 **Statistics**

398 Statistical analyses were carried out using GraphPad Prism (8.4.1). Data were presented in mean ±
399 standard deviation in **Figure 3,** and in mean ± standard error in **Supplementary Figure 4**. For comparing
400 normalized vessel diameter time-lapse traces (**Figure 3e** and **4d**), Student's t-test was performed with
401 each timepoint, with Bonferroni correction for multiple comparison. For comparing the two-photon
402 mediated vessel motility in different conditions, one-sample Wilcoxon tests were used for each group to
403 compare to a value of 1 (**Figure 3f** and **4e**) or 0 (**Figure 3g**), with additional Bonferroni's correction for
404 multiple comparison. For comparing the efficacy of neuronal optogenetics with and without
405 fluorescence transfer (**Supplementary Figure 4e**), we fit the response probability from each group to the
406 following exponential equation: Y = 1-exp(-K*(X-L), in which the parameter L indicates the minimal
407 power to elicit calcium responses and K indicates the change rate of the curve. Extra sum-of-squares F
408 test was used to determine whether two sets of parameters were statistically different.

409

410 **Data availability**

411 All data presented show individual data points whenever possible to facilitate replication of our graphs
412 and associated statistics. All raw images and recording data are available upon request.

413

414 **Code availability**

415 All equations for modeling calculations were presented in figures. All data processing steps in the study
416 used standard built-in functions that should be self-explanatory. The scripts used for analyzing calcium
417 responses are included in **Supplementary Material**. We will provide any additional details of the
418 functions upon request.

419

420 References:

421 1. Boyden ES, Zhang F, Bamberg E, Nagel G, Deisseroth K. Millisecond-timescale, genetically targeted
422 optical control of neural activity. NAT NEUROSCI. 2005 2005-01-01;8(9):1263-8.

423 2. Deisseroth K. Optogenetics. NAT METHODS. 2011 2011-01-01;8(1):26-9.

424 3. Oron D, Papagiakoumou E, Anselmi F, Emiliani V. Two-photon optogenetics. PROG BRAIN RES. 2012
425 2012-01-01;196:119-43.

426 4. Prakash R, Yizhar O, Grewe B, Ramakrishnan C, Wang N, Goshen I, et al. Two-photon optogenetic
427 toolbox for fast inhibition, excitation and bistable modulation. NAT METHODS. 2012 2012-01-01;9(12):1171-9.

428 5. Carrillo-Reid L, Yang W, Bando Y, Peterka DS, Yuste R. Imprinting and recalling cortical ensembles.
429 SCIENCE. 2016 2016-01-01;353(6300):691-4.

430 6. Shemesh OA, Tanese D, Zampini V, Linghu C, Piatkevich K, Ronzitti E, et al. Temporally precise single-
431 cell-resolution optogenetics. NAT NEUROSCI. 2017 2017-01-01;20(12):1796-806.

432 7. Mardinly AR, Oldenburg IA, Pégard NC, Sridharan S, Lyall EH, Chesnov K, et al. Precise multimodal
433 optical control of neural ensemble activity. NAT NEUROSCI. 2018 2018-01-01;21(6):881-93.

434 8. Zhang Z, Russell LE, Packer AM, Gauld OM, Häusser M. Closed-loop all-optical interrogation of neural
435 circuits in vivo. NAT METHODS. 2018 2018-01-01;15(12):1037-40.

436 9. Rickgauer JP, Tank DW. Two-photon excitation of channelrhodopsin-2 at saturation. P NATL ACAD SCI
437 USA. 2009 2009-01-01;106(35):15025-30.

438 10. Zhu P, Narita Y, Bundschuh ST, Fajardo O, Schärer YZ, Chattopadhyaya B, et al. Optogenetic Dissection
439 of Neuronal Circuits in Zebrafish using Viral Gene Transfer and the Tet System. FRONT NEURAL CIRCUIT.
440 2009;3:21.

441 11. Andrasfalvy BK, Zemelman BV, Tang J, Vaziri A. Two-photon single-cell optogenetic control of neuronal
442 activity by sculpted light. P NATL ACAD SCI USA. 2010;107(26):11981-6.

443 12. Papagiakoumou E, Anselmi F, Bègue A, de Sars V, Glückstad J, Isacoff EY, et al. Scanless two-photon
444 excitation of channelrhodopsin-2. NAT METHODS. 2010;7(10):848-54.

445 13. Denk W, Strickler JH, Webb WW. Two-photon laser scanning fluorescence microscopy. SCIENCE. 1990
446 1990-01-01;248(4951):73-6.

447 14. Wells J, Kao C, Mariappan K, Albea J, Jansen ED, Konrad P, et al. Optical stimulation of neural tissue in
448 vivo. OPT LETT. 2005 2005-01-01;30(5):504-6.

449 15. Rungta RL, Osmanski B, Boido D, Tanter M, Charpak S. Light controls cerebral blood flow in naive
450 animals. NAT COMMUN. 2017 2017-01-01;8:14191.

451 16. Walsh AJ, Tolstykh GP, Martens S, Ibey BL, Beier HT. Action potential block in neurons by infrared light.
452 NEUROPHOTONICS. 2016 2016-01-01;3(4):40501.

453 17. Picot A, Dominguez S, Liu C, Chen I, Tanese D, Ronzitti E, et al. Temperature Rise under Two-Photon
454 Optogenetic Brain Stimulation. CELL REP. 2018 2018-01-01;24(5):1243-53.

455 18. Owen SF, Liu MH, Kreitzer AC. Thermal constraints on in vivo optogenetic manipulations. NAT
456 NEUROSCI. 2019 2019-01-01;22(7):1061-5.

457 19. Davalos D, Grutzendler J, Yang G, Kim JV, Zuo Y, Jung S, et al. ATP mediates rapid microglial response
458 to local brain injury in vivo. NAT NEUROSCI. 2005 2005-01-01;8(6):752-8.

459 20. Zeng X, Bhasin S, Wu X, Lee J, Maffi S, Nichols CJ, et al. Hsp70 dynamics in vivo: effect of heat shock
460 and protein aggregation. J CELL SCI. 2004 2004-01-01;117(Pt 21):4991-5000.

461 21. Duke CG, Savell KE, Tuscher JJ, Phillips RA, Day JJ. Blue Light-Induced Gene Expression Alterations in
462 Cultured Neurons Are the Result of Phototoxic Interactions with Neuronal Culture Media. eNeuro. 2020 2020-01-
463 01;7(1).

464 22. Hernandez O, Papagiakoumou E, Tanese D, Fidelin K, Wyart C, Emiliani V. Three-dimensional
465 spatiotemporal focusing of holographic patterns. NAT COMMUN. 2016 2016-01-01;7:11928.

466 23. Pégard NC, Mardinly AR, Oldenburg IA, Sridharan S, Waller L, Adesnik H. Three-dimensional scanless
467 holographic optogenetics with temporal focusing (3D-SHOT). NAT COMMUN. 2017 2017-01-01;8(1):1228.

468 24. Carrillo-Reid L, Han S, Yang W, Akrouh A, Yuste R. Controlling visually guided behavior by holographic
469 recalling of cortical ensembles. CELL. 2019 2019-01-01;178(2):447-57.

470 25. Marshel JH, Kim YS, Machado TA, Quirin S, Benson B, Kadmon J, et al. Cortical layer-specific critical
471 dynamics triggering perception. SCIENCE. 2019 2019-01-01;365(6453).

472 26. Rickgauer JP, Deisseroth K, Tank DW. Simultaneous cellular-resolution optical perturbation and imaging
473 of place cell firing fields. NAT NEUROSCI. 2014;17(12):1816-24.

474 27. Packer AM, Russell LE, Dalgleish HWP, Häusser M. Simultaneous all-optical manipulation and recording
475 of neural circuit activity with cellular resolution in vivo. NAT METHODS. 2015;12(2):140-6.

476 28. Webb RC. Smooth muscle contraction and relaxation. ADV PHYSIOL EDUC. 2003 2003-01-01;27(1-
477 4):201-6.

478 29. Hill RA, Tong L, Yuan P, Murikinati S, Gupta S, Grutzendler J. Regional blood flow in the normal and
479 ischemic brain is controlled by arteriolar smooth muscle cell contractility and not by capillary pericytes. NEURON.
480 2015 2015-01-01;87(1):95-110.

481 30. Mateo C, Knutsen PM, Tsai PS, Shih AY, Kleinfeld D. Entrainment of Arteriole Vasomotor Fluctuations
482 by Neural Activity Is a Basis of Blood-Oxygenation-Level-Dependent "Resting-State" Connectivity. NEURON.
483 2017 2017-01-01;96(4):936-48.

484 31. Hartmann DA, Berthiaume A, Grant RI, Harrill SA, Koski T, Tieu T, et al. Brain capillary pericytes exert a
485 substantial but slow influence on blood flow. NAT NEUROSCI. 2021;24(5):633-45.

486 32. Tong L, Hill RA, Damisah EC, Murray KN, Yuan P, Bordey A, et al. Imaging and optogenetic modulation
487 of vascular mural cells in the live brain. NAT PROTOC. 2021;16(1):472-96.

488 33. Mohanty SK, Reinscheid RK, Liu X, Okamura N, Krasieva TB, Berns MW. In-depth activation of
489 channelrhodopsin 2-sensitized excitable cells with high spatial resolution using two-photon excitation with a near-
490 infrared laser microbeam. BIOPHYS J. 2008 2008-01-01;95(8):3916-26.

491 34. Han X, Chow BY, Zhou H, Klapoetke NC, Chuong A, Rajimehr R, et al. A high-light sensitivity optical
492 neural silencer: development and application to optogenetic control of non-human primate cortex. Frontiers in
493 Systems Neuroscience. 2011 2011-01-01;5:18.

494 35. Chaigneau E, Ronzitti E, Gajowa MA, Soler-Llavina GJ, Tanese D, Brureau AYB, et al. Two-Photon
495 Holographic Stimulation of ReaChR. FRONT CELL NEUROSCI. 2016 2016-01-01;10:234.

496 36. Drobizhev M, Makarov NS, Tillo SE, Hughes TE, Rebane A. Two-photon absorption properties of
497 fluorescent proteins. NAT METHODS. 2011 2011-01-01;8(5):393-9.

498 37. Drobizhev M, Tillo S, Makarov NS, Hughes TE, Rebane A. Absolute two-photon absorption spectra and
499 two-photon brightness of orange and red fluorescent proteins. The Journal of Physical Chemistry. B. 2009 2009-01-
500 01;113(4):855-9.

501 38. Lin JY. A user's guide to channelrhodopsin variants: features, limitations and future developments. EXP
502 PHYSIOL. 2011 2011-01-01;96(1):19-25.

503 39. Lin JY, Knutsen PM, Muller A, Kleinfeld D, Tsien RY. ReaChR: a red-shifted variant of channelrhodopsin
504 enables deep transcranial optogenetic excitation. NAT NEUROSCI. 2013 2013-01-01;16(10):1499-508.

505 40. Cherkas V, Grebenyuk S, Osypenko D, Dovgan AV, Grushevskyi EO, Yedutenko M, et al. Measurement
506 of intracellular concentration of fluorescently-labeled targets in living cells. PLOS ONE. 2018 2018-01-
507 01;13(4):e194031.

508 41. Yang W, Carrillo-Reid L, Bando Y, Peterka DS, Yuste R. Simultaneous two-photon imaging and two-
509 photon optogenetics of cortical circuits in three dimensions. ELIFE. 2018 2018-01-01;7.

510 42. Zipfel WR, Williams RM, Webb WW. Nonlinear magic: multiphoton microscopy in the biosciences. NAT
511 BIOTECHNOL. 2003 2003-01-01;21(11):1369-77.

512 43. Chen F, LoTurco J. A method for stable transgenesis of radial glia lineage in rat neocortex by piggyBac
513 mediated transposition. J NEUROSCI METH. 2012 2012-01-01;207(2):172-80.

514 44. Hill RA, Damisah EC, Chen F, Kwan AC, Grutzendler J. Targeted two-photon chemical apoptotic ablation
515 of defined cell types in vivo., 2017. p. 15837.

516 45. Ting JT, Lee BR, Chong P, Soler-Llavina G, Cobbs C, Koch C, et al. Preparation of Acute Brain Slices
517 Using an Optimized N-Methyl-D-glucamine Protective Recovery Method. Journal of Visualized Experiments. 2018
518 2018-01-01(132).

519 46. Mütze J, Iyer V, Macklin JJ, Colonell J, Karsh B, Petrášek Z, et al. Excitation spectra and brightness
520 optimization of two-photon excited probes. BIOPHYS J. 2012;102(4):934-44.

521

522 **Acknowledgement**

523 We thank Dr. Oscar Hernandez (Stanford University) for his guidance on the estimation of fluorescence
524 irradiance by two-photon excitation, and Dr. Jonathan Demb (Yale University) for helpful conceptual and
525 technical discussions. This work was supported by NIH R01NS115544 (J.G.). J.B. was additionally
526 supported by NIH R01GM118486. M.C. and Z.J.Z were additionally supported by NIH R01EY026065 (ZJZ),
527 P30EY026878 (Yale Vision Core). P.Y. was additionally supported by startup fund IDF2641002 (Fudan
528 University).

529

530 **Author contributions**

531 P.Y and J.G. designed the study. L.T., P.Y. and F.C. carried out the experiments. P.Y. and J.B. performed
532 theoretical calculations. Y.X., M.C. and J. Z. performed the electrophysiology recording. P.Y., L.T. and J.G.
533 wrote and edited the manuscript.

534

535 **Competing interests**

536 The authors declare no competing interests.

537

Single cell in vivo brain optogenetic stimulation by two-photon excitation fluorescence transfer

Lei Tong*[1], Peng Yuan*[1,2,#], Yao Xue[3], Minggang Chen[3], Fuyi Chen[1], Joerg Bewersdorf[5,6], Z. Jimmy Zhou[3,4,7], Jaime Grutzendler[1,4.#]

1, Department of Neurology, Yale School of Medicine, New Haven, CT, 06511

2, Department of Rehabilitation Medicine, Huashan Hospital, State Key Laboratory of Medical Neurobiology, Institute for Translational Brain Research, MOE Frontiers Center for Brain Science, Fudan University, Shanghai 200032, China

3, Department of Ophthalmology and Visual Science, Yale School of Medicine, New Haven, CT, 06511

4, Department of Neuroscience, Yale School of Medicine, New Haven, CT, 06511

5, Department of Cell Biology, Yale School of Medicine, New Haven, CT, 06511

6, Department of Biomedical Engineering, Yale University, New Haven, CT, 06511

7. Department of Cellular and Molecular Physiology, Yale University, New Haven, CT, 06511

*, authors contributed equally to this work

#, corresponding author

Supplementary Material

In some cases, the DNA sequences encoding the target proteins (tagBFP, tdTomato and ReaChR) were cloned from the original constructs into an AAV-CAG backbone (the backbone was acquired from Addgene #28014, deleting the GFP sequence), and the resulted plasmids were used for in utero electroporation. Standard molecular cloning procedures were performed using the following reagents: Phusion High-Fidelity DNA Polymerase (New England BioLabs, M0530S), Restriction enzymes (New England BioLabs), T4 DNA ligase (ThermoFisher Scientific, EL0011), QIAGEN plasmid Maxi kit (#12162). All modified constructs were sequences to verify the correct insertion and sequence. The modified plasmid maps are showed below:

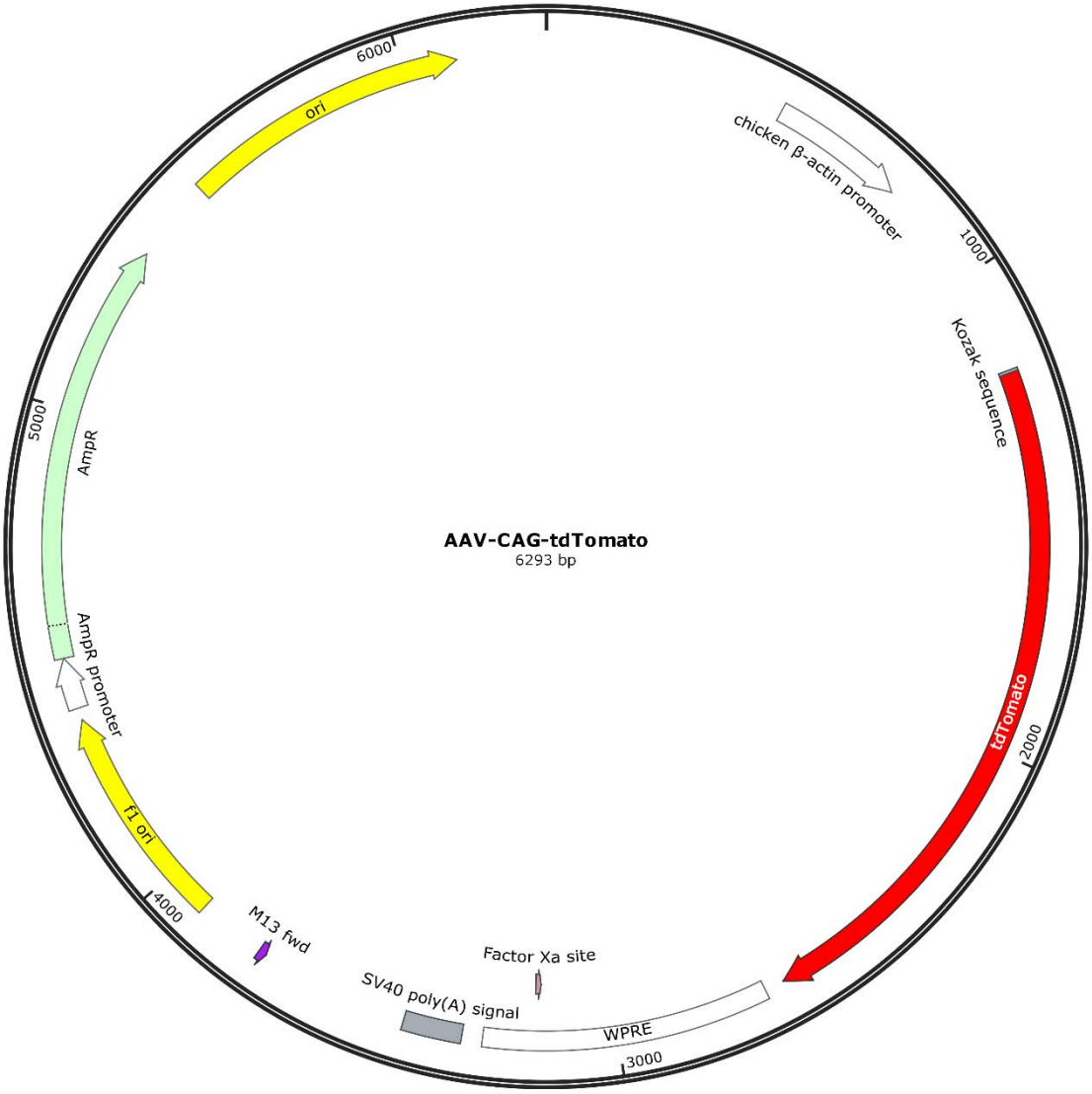
AAV-CAG-tdTomato
6293 bp
chicken β-actin promoter
Kozak sequence
tdTomato
WPRE
Factor Xa site
SV40 poly(A) signal
M13 fwd
f1 ori
AmpR promoter
AmpR
ori
1000
2000
3000
4000
5000
6000

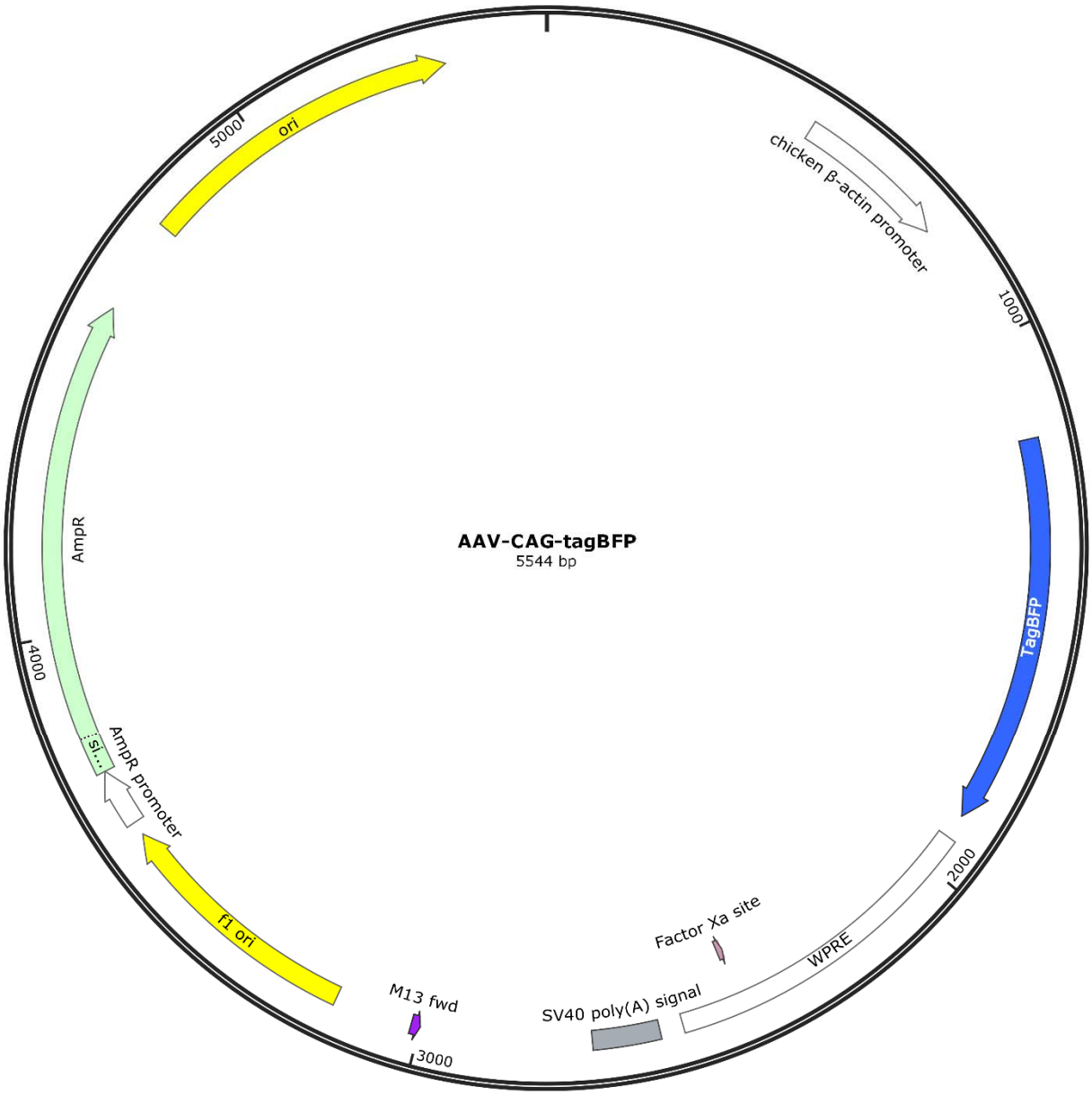
AAV-CAG-tagBFP
5544 bp
ori
5000
chicken β-actin promoter
1000
TagBFP
2000
WPRE
Factor Xa site
SV40 poly(A) signal
M13 fwd
3000
f1 ori
AmpR promoter
AmpR
4000

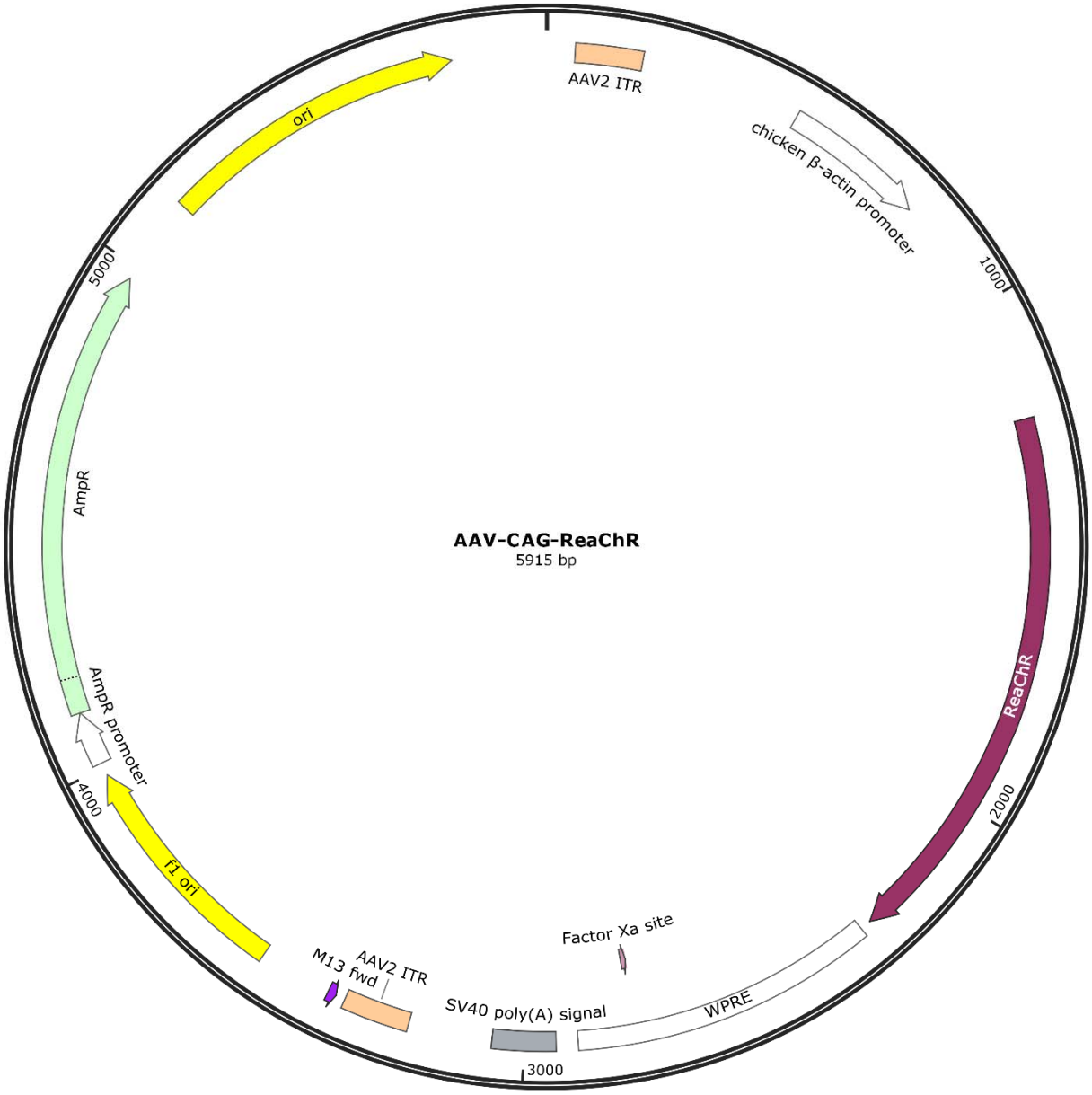

Custom scripts for analyzing calcium responses

We used MATLAB for this part of the analysis.

```
%%
clearvars; close all;
[title,path] = uigetfile('*.xml','Select the image file');
cd(path);
text = fileread(title);
```

```
% Find dimensions of 5D image
% XY dimensions: Entries assumed to be the same for pixel dimensions
xdim = str2double(regexp(text, ...
   'PVStateValue key="pixelsPerLine".*?value="(\d*)"', 'tokens','once'));
ydim = str2double(regexp(text, ...
   'PVStateValue key="linesPerFrame".*?value="(\d*)"', 'tokens','once'));

% Z axis dimension
z_cell =  regexp(text, 'Frame relative.*?index="(\d*)"', 'tokens');
zslice = cellfun(@(x) str2double(x{1}),z_cell);

% T axis dimension
t_cell =  regexp(text, 'Sequence type=.*?cycle="(\d*)"', 'tokens');
tpoints = cellfun(@(x) str2double(x{1}),t_cell);
if tpoints == 0; tpoints=1; end
t = cellfun(@str2double, regexp(text, ...
   'Frame relativeTime="(\d+(\.\d*)|0)"', 'tokens','all'))';

% Channel dimension (img names found on same line, parsed also)
ch_img_names_cell =  regexp(text, ...
   'File channel="(\d*)".*?filename="(.*?)"', 'tokens');
ch = cellfun(@(x) str2double(x{1}),ch_img_names_cell);
img_names = cellfun(@(x) x{2},ch_img_names_cell, 'UniformOutput', 0);

% Bit depth of img in filesystem
tif_bit_depth = str2double(regexp(text, ...
   '<PVStateValue key="bitDepth".*?value="(\d*)"', 'tokens','once'));

% Create 1x1 mapping between img_name, channel, z slice, timepoint
% Channel index
ch_ind = ch;

% Zslice and timpoint index need to be repeated to match img_names elements
flat = @(x) x(:);
z_ind = flat(repmat(zslice, [numel(unique(ch_ind)) 1]));
t_ind = flat(repmat(tpoints, [numel(unique(z_ind))*numel(unique(ch_ind)) 1]));


% Initialize image specified datatype
xyczt_img = zeros(ydim, xdim, max(ch), ...
   max(zslice), max(tpoints), 'uint16');

% Read individual tif files into 5D img
for n = 1:numel(img_names)
   xyczt_img(:,:,ch_ind(n), z_ind(n), t_ind(n)) = imread(img_names{n})...
   * double(intmax('uint16')/2^tif_bit_depth);
end

clearvars -except xyczt_img t;
temp = xyczt_img(:,:,:,:,2);
xyczt_img = temp;

%%
% ROI of the neuron, BFP run this section
bw = imbinarize(imgaussfilt(mat2gray(xyczt_img(:,:,4,1)),2),0.4);
figure,imshowpair(mat2gray(xyczt_img(:,:,4,1)),bw.*0.5);
bw = repmat(bw,[1 1 size(xyczt_img,4)]);
```

```
%% ROI of the neuron, tdTomato run this section
bw = imbinarize(imgaussfilt(mat2gray(xyczt_img(:,:,2,1)),2),0.2);
figure,imshowpair(mat2gray(xyczt_img(:,:,4,1)),bw.*0.5);
bw = repmat(bw,[1 1 size(xyczt_img,4)]);


%%
rcamp = squeeze(xyczt_img(:,:,2,:));
intensity = mean(reshape(rcamp(bw),[],size(xyczt_img,4)));
gfp = squeeze(xyczt_img(:,:,4,:));
intensity_gfp = mean(reshape(gfp(bw),[],size(xyczt_img,4)));
intensity = intensity./intensity_gfp.*mean(intensity_gfp);
intensity_m = intensity'./mean(intensity(1:10))-1;
figure,plot(intensity_m);
num2clip(intensity');

%%
[xData, yData] = prepareCurveData(t(1:150), intensity_m(1:150));
ft = fittype('poly1');
[fitresult, gof] = fit(xData, yData, ft);
p = coeffvalues(fitresult);p(1)
```

Supplementary Figures

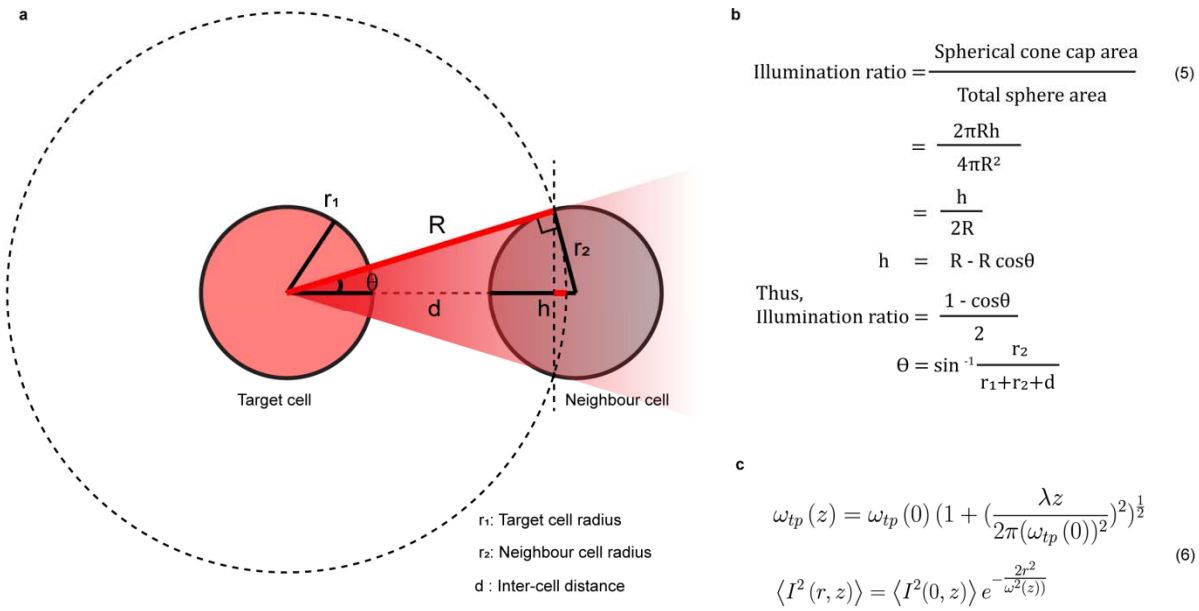

Supplementary Figure 1: Estimation of the TEFT illumination to a neighboring cell.

(**a**) A 2-dimensional schematic illustrating the illumination to the target cell and to the neighbor cell. The total flux through any spherical surface enclosing the fluorescence emission volume is the same and can be considered 100% of the spherical surfaces, while only a cone of the original spherical emission sphere will irradiate a neighboring cell (red cone). (**b**) Equations for calculating the illumination ratio between the target cell and the neighbor cell. The illumination ratio equals to the ratio between the spherical cone cap area and the total sphere area. Results are presented in **Figure 2i**. (**c**) Equations for calculating the out-of-focus two-photon effect along the axial direction for **Figure 2h**.

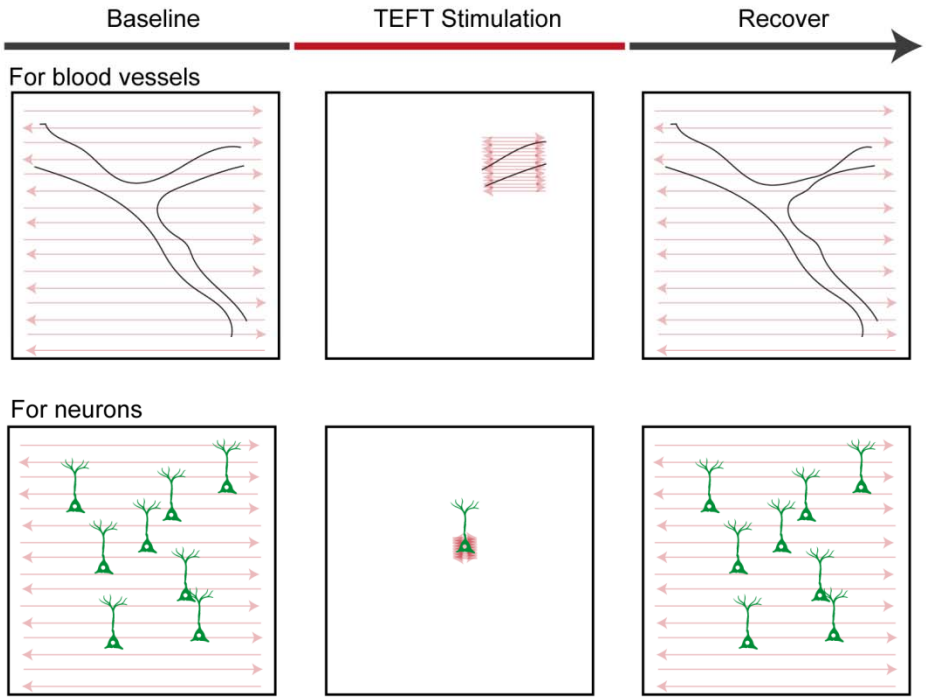

Supplementary Figure 2: Schematics of the TEFT-imaging protocol used in this study.

We implemented a 3-stage imaging protocol to achieve recording and TEFT stimulation. At baseline, the galvanometer was set to full range with low laser power (controlled by a pockel cell). This allowed us to image the target and the surrounding regions without causing activation of the opsin. To achieve TEFT stimulation, we limited the scanning to the location of the target structure with the laser power required for stimulation. We were able to image the target structure during this period. At the end of the stimulation period, the scanning and laser were set back to the same conditions as the baseline stage, and at this point we went on to record the morphology and activity of the same region after stimulation.

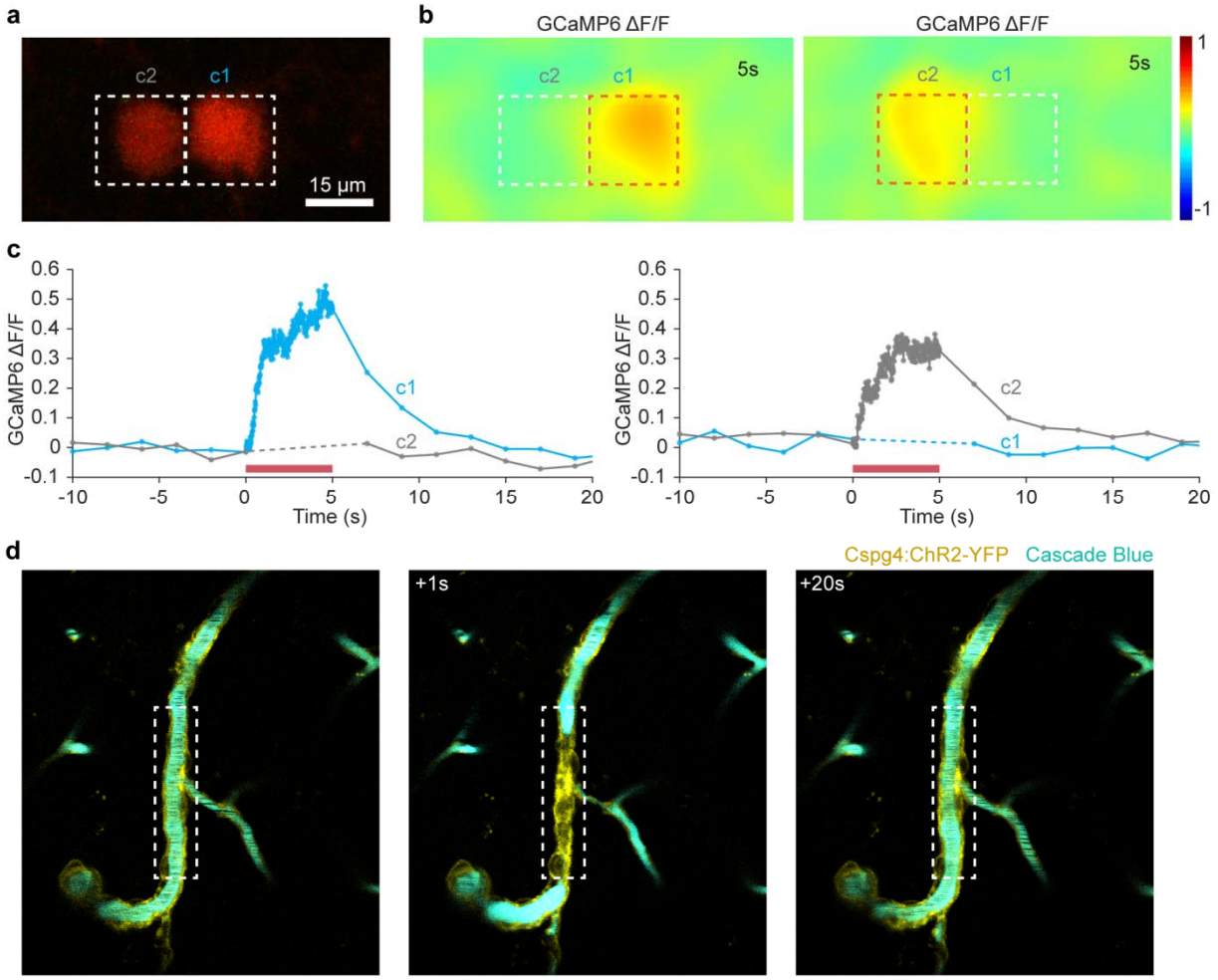

Supplementary Figure 3: Fluorescence transfer-mediated two-photon stimulation retains high spatial resolution in vivo.

(**a**) Sequential two photon stimulation (920nm) of single neuron out of two adjacent ReaChR, GCaMP6 and tdTomato coexpressing cells (top-left). (**b**) Heat maps of individual cell GCaMP6 responses immediately after excitation of a ROI positioned on the stimulated neuron (orange dashed box; middle and -right panels). (**c**) Calcium response curves of these two neurons (Dotted line indicates interval without scanning, see methods for detail) using stimulation parameters as in **a**, show that despite their proximity, the tdTomato emission within the illuminated ROI from either cell is unable to activate the immediately adjacent cell, highlighting the preservation of spatial specificity when using two photon florescence transfer optogenetics. (**d**) Two-photon time-lapse images of vessel constriction in a Cspg4-cre:Ai32 mouse with intravascular blue dye. White dashed boxes indicated the stimulation scanning region of interest. Notice the restriction of the constricted area to the illumination ROI only. Quantification of these data are presented in **Figure 3g**.

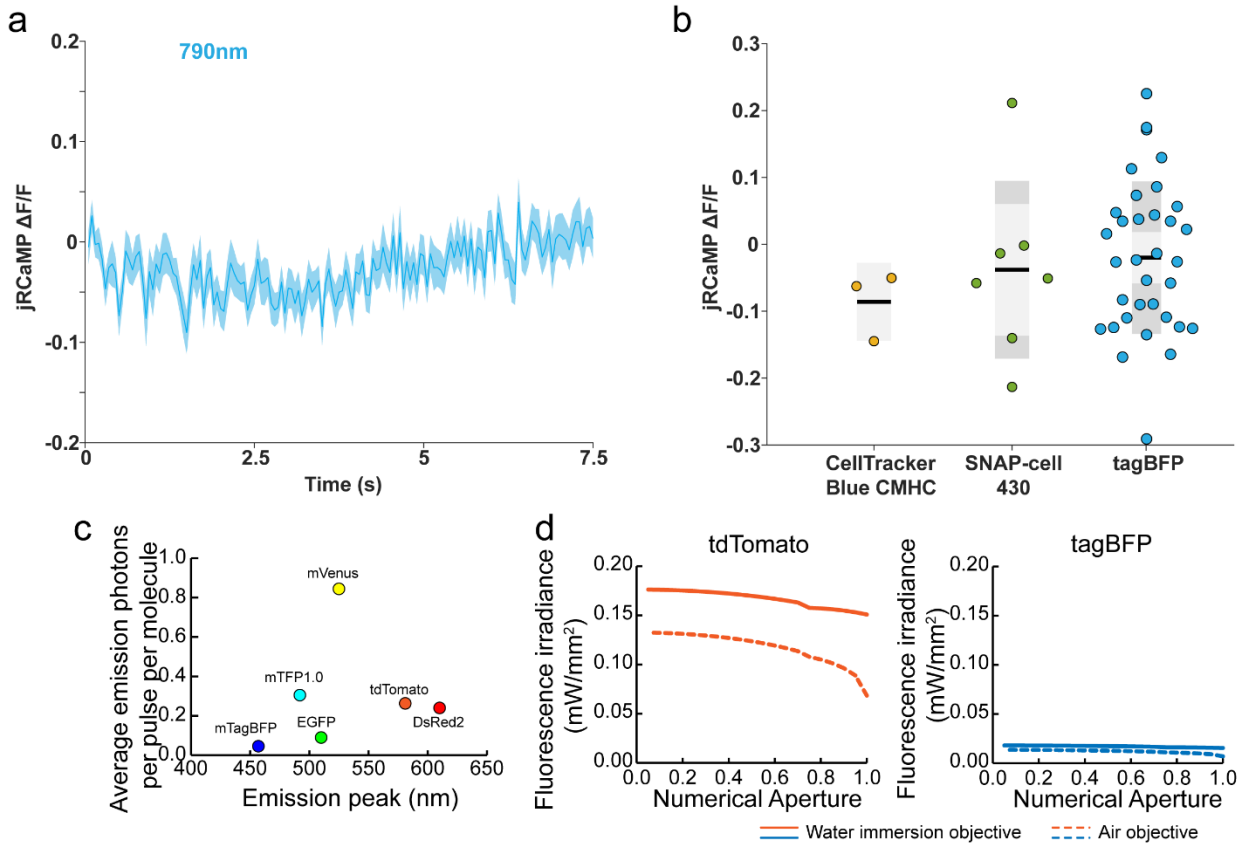

Supplementary Figure 4: Ineffective excitation of ChR2 in neurons using blue fluorescent proteins reveal critical constraints for optimal TEFT efficiency. (**a**) Calcium response of ChR2, jRCaMP and tagBFP positive neurons (N=34) shows no response when scanned with two-photon (780 nm for tagBFP excitation, 1045 nm for jRCaMP calcium imaging, 4 µs dwell time, ~15 mW); ROI scanning (48x48 pixels, 20 Hz, for 5 s) performed on the neuron soma. Data are represented as mean ± standard error. (**b**) Quantification of calcium response during two-photon scanning (similar to **a**) with CellTracker Blue CMHC, SNAP-cell 430, and tagBFP in ChR2 and jRCaMP co-expressing neurons (N=3, N=7, N=34). Data are represented as mean ± standard error. An important note is that none of the organic dyes or SNAP-cell 430 labeling strategies achieved sufficiently bright labeling in vivo, potentially limiting the overall stimulation efficiency. (**c**) Theoretical calculations of two-photon fluorescence photon generation for selected fluorescent proteins using the equation in **Figure 2**. Two-photon excitation wavelengths used in calculations corresponded to the peak cross-section of each protein. Laser power was kept at 10 mW with a 1.0 numerical aperture lens. (**d**) Estimations of two-photon excitation fluorescence irradiance of tdTomato and tagBFP, with various objectives (air or water immersion, numerical aperture from 0.05-1.0). Laser power was kept at 10 mW, fluorescent protein concentration was set at 10 µM, and a target cell was 5 µm in diameter. Based on these calculations the blue-emitting proteins have a theoretical low efficiency for exciting the opsins, consistent with our experimental data.

Supplementary Discussion

We would like to provide an additional discussion regarding whether the red fluorescent protein commonly fused with opsins would be a potent TEFT source, as this question has been brought up multiple times from several readers.

It is important to recognize that the 1:1 ratio between opsin and fluorphore and their location on the membrane both limit the generation of sufficient photons. In fact, the dense packing of fluorescent proteins is a key factor for the efficiency of the TEFT method.

To illustrate this point, here we described a back-of-envelope calculation to put this into proper scale. The key issue is that a fusion protein cannot provide enough photons to induce the TEFT effect.

For TEFT illumination, we used the parameters described in **Figure 2f**:

Two-photon focal volume: 0.28×10^{-15} L, fluorophore concentration: 10 µM, this leads to a total of 1686 molecules stimulated at each pulse of two-photon excitation.

Number of molecules = focal volume x concentration x Avogadro's number

$$= 0.28 \times 10^{-15} \times 10 \times 10^{-6} \times 6.02 \times 10^{23}$$

$$\approx 1686$$

For membrane fusion, the expression of opsins can be ranging from 90 - 750 molecules per μm^2 [1,2]. Given the ~0.2 µm XY-plane resolution, the activated molecules on the membrane are fewer than 30, which is about 2 orders of magnitude lower than the TEFT methods. In fact, the estimated total density of membrane proteins is about 30000 molecules per μm^2 [1], and usually the overexpression of exogenous proteins will be ~2-3 % of this value. Even if we are assuming very generously that the opsin expression constitutes 10% of total membrane protein, which is never achieved, we are still only activating ~120 molecules at each moment, which is one order of magnitude lower than our TEFT method.

References:

[1] Quinn, P., Griffiths, G. & Warren, G., Density of newly synthesized plasma membrane proteins in intracellular membranes II. Biochemical studies. *The Journal of cell biology* **98** 2142 (1984).

[2] Nagel, G., Möckel, B., Büldt, G. & Bamberg, E., Functional expression of bacteriorhodopsin in oocytes allows direct measurement of voltage dependence of light induced H+ pumping. *FEBS LETT* **377** 263 (1995).